Journal of Biometrics & Biostatistics

Review Article Open Access

Statistics in Bioarcheology: A Review

Clifford Qualls[1] **and Otto Appenzeller**[2,3*]

[1]*Health Sciences Center, University of New Mexico, Albuquerque, NM, USA*
[2]*New Mexico Health Enhancement and Marathon Clinics (NMHEMC) Research foundation, Albuquerque, NM 87122, USA*
[3]*New Mexico Museum of Natural History and Science Albuquerque NM 87104, USA*

Abstract

Statistics is a branch of mathematics dealing with the collection, analysis, interpretation, and presentation of numerical data, whereas, mummy studies are about death and mortality in ancient populations. The combination of an exact science (statistics) together with attempts at the restoration of the biology of long dead individuals requires interpretation of statistical data and knowledge of biology. Here we review recent progress made in this field.

Bioarcheology relies on statistical modeling. These are mathematical models that embody a set of statistical assumptions concerning the generation of some sample data from a larger population. A statistical model represents a form of the data. The assumptions used in statistical models describe probability distributions, from which a particular data set is sampled. These probability distributions distinguish a statistical model from other, non-statistical, mathematical models. The statistical models are best represented by mathematical equations.

Keywords: Bioarcheology; Statistics; Mathematical models; Population

Statistical Methods in Bioarcheology

T-test

Tooth growth is essential to health and survival. In humans the growth rate can be inferred from the width of perikymata growth intervals. We measured the intervals between perikymata ridges on the surfaces of teeth and in thin sections of molars of modern human molars (which we used as standards), in ancient, prehistoric and modern humans. We compared statistically the results from ancient and prehistoric teeth to modern teeth and assessed the impact of dietary factors and sociality (sociality is the degree to which individuals in an animal (or human) population tend to associate in social groups) on tooth growth. We found that ancient teeth grew faster than modern teeth (wider intervals) because of environmental, nutritional and life style influences. This apparently conferred evolutionary advantages for human survival. We used the t-test to model our results.

The t-test is any statistical hypothesis test in which the test statistic follows a Student's t-distribution under the null hypothesis. A t-test is commonly applied when the test statistic would follow a normal distribution if the value of a scaling term in the test statistic were known. Examples used in bioarcheology can be found in reference [1].

Anova

Paleopathology is a well-established science. By contrast, paleoneurobiology, a term encompassing the study of neural tissues from mummified remains, is almost non-existent. This is partly due to the poor preservation of neural tissues by natural or artificial mummification. Recognizing neurological diseases in ancient humans is, however, possible by scrutiny of their portraits and comparing the images to surviving skeletal remains. Painted portraits of Egypt's Roman period have survived and have been called "the most remarkable products of the ancient world". These portraits, many of great artistic merit, were painted about 2000 years ago; they were part of the funerary practices in northern Egypt and arose in response to a concern for the wellbeing of the dead. One feature of Egyptian civilization was the conviction that life after death was inevitable. To survive death and thereby facilitate the transition to the next life required a passage from earthly to the other life in both spiritual and physical forms. The corpse was preserved by mummification because of a concern for the wellbeing of the dead.

The funerary portraits were commemorative expressions of respect for distinguished citizens at Rome. During the Republic these portraits were restricted to the nobility and to the families of serving magistrates. By the time of the Roman Empire the portraits were no longer restricted by class but became a means of proclaiming loyalty to the reigning emperor [2].

About 200 mummy portraits painted in color at the beginning of the first millennium were examined. Thirty two skulls excavated at Hawara in the Fayum (northern Egypt), where most of the portraits were found were measured, and nine caliper measures on each side of the skulls were taken. The right/left ratios were analyzed by analysis of variance (ANOVA).

Time series

We review methods used in analyses of archeological data of human and vertebrate animals. The remains of human and vertebrate animals consist of bone, teeth or hair; each show growth increments and each can be measured for isotope ratios and other chemicals in equal intervals along the direction of growth. Both growth increments and chemical assay in equal intervals give rise to (discrete-time) time series where measurements are $Y_1, Y_2, \cdots Y_N$ and N is the length of the series. An analysis of time series can be a spectral analysis where the series is decomposed into a linear combination of sines or cosines; the spectra is a list or plot of amplitudes versus frequencies. An analysis of the spectra is said to be done in the frequency domain. A definition of the spectrum (periodogram) $I(\lambda)$ is:

$$I(\lambda) = \frac{1}{2\pi N}\left|\sum_{t=1}^{N} Y(t)\, e^{-i\lambda t}\right|^2, \; for -\pi < \lambda \le \pi,$$

***Corresponding author:** Otto Appenzeller, New Mexico Health Enhancement and Marathon Clinics (NMHEMC) Research foundation, Albuquerque, NM 87122, USA, Tel: 5517-981666732; E-mail: ottoarun12@aol.com

Received February 01, 2019; **Accepted** February 15, 2019; **Published** February 20, 2019

Citation: Qualls C, Appenzeller O (2019) Statistics in Bioarcheology: A Review. J Biom Biostat 10: 421.

That can be computed by the Fast Fourier Transform. Here the $e^{-i\lambda t}$ is complex form $cos(\lambda t) + i\ sin(\lambda t)$ with $i = \sqrt{-1}$ and t is the times and λ is the list of frequencies. The addition of the annual growth rate to the spectral information allows the frequencies to be interpreted as periodicities in units of time (year).

Another analysis of time series can be done in the time domain where one analyzes the time series directly; such as fitting a seasonal component. The traditional cosinor analysis (regression versus time) is an example; time domain calculations are used to remove an annual sinusoid, which was done as a preliminary step in the analysis of hair from mammoths [3].

The autoregressive model AR(k) model of order k is:

$Y_i = \beta_{i-1}Y_{i-1} + \beta_{i-2}Y_{i-2} + \cdots \beta_{i-k}Y_{i-k} + \varepsilon$, from which a spectral density can be computed. More generally, AutoRegressive-Integrated-Moving Average (ARIMA) models which include the AR model could be used. These analyses are linear; below we also give one form of non-linear analysis, Approximate Entropy (ApEN).

Spectral peaks

The energy necessary for life and its rhythms is provided by metabolism. The changes in metabolism induced by the sun are synchronous with the sun rising every 24 hours, that is they are circadian (~24 hours). We showed that biologic rhythms can be derived from fossil imprints left in rock formations of feathered creatures that lived millions of years ago. We compared the imprints of feathers' growth lines that measure circadian growth from the past with the corresponding measurements from extant birds. Circadian rhythms are biological cycles such as temperature fluctuations recurring approximately every 24 hours synchronous with celestial events that are predicated by the rotation of the earth around the sun. Such cycles are ubiquitous in living beings from unicellular protists living in the sea to giants such as extant elephants and whales to even titanic creatures such as extinct Sauropod dinosaurs.

Daily growth lines were measured in 9 photographs of dinosaur feather-imprints. They were from an enantiornithine bird (Mesozoic 245-265 million years), from a troodontid theropod (Cretaceous ~160 million years) and from Sinosauropteryx (Early Cretaceous; ~125 million years; rachis only). We measured 27 growth lines and 39 rachis intervals in the turkey feather. We compared our measurements in the dinosaurs to those in the modern feather. We used biometrics to analyze the measurements, we found circadian and multidien rhythms in all feathers. The gliding Microraptor had large feathers. In contrast, the feathered dinosaurs had smaller feathers. Wild turkey feathers were of intermediate size.

Based on measurements and statistically identified spectral peaks, we find circadian and multidien rhythms in feather imprints of dinosaurs and in extant birds similar to those described in mammals. Feather growth is related to metabolism, to function and to body mass; this suggests a similar metabolism existed in feathered dinosaurs and modern birds. Thus statistical modeling allowed us to deduce the metabolism of long extinct feathered dinosaurs [4].

Nyquist Folding Frequency

The interpretation of spectral peaks can be confounded by the Nyquist folding frequency. Forensic time series are not measured continuously and the use of Δt affects the computed spectral density; one cannot hope to measure frequencies higher than a certain value taking place within an interval of length Δt. Furthermore, the spectral density is folded over at the Nyquist folding frequency ω_N with the high frequency content above ω_N being added to the low frequency content below ω_N. For the Smithsonian mammoth hair [3,14], we have

$$\textit{Nyquist folding frequency} \quad \omega_N = \frac{.5}{\Delta t} = \frac{.5\ cycles / obs}{0.3\ cm / obs} = 1.67 cycles / \text{cm}.$$

This folding frequency times the growth rate gives a frequency of 1.03 cycles/week with a corresponding periodicity of 1/1.03 or approximately 1.0 week. Since we are not examining periodicities this low or lower, there may be no fold-back contamination in the results. We have excluded the daily cycles from our interest; a much smaller Δt would have been necessary for this purpose. Though we are not examining the daily cycles directly, it could be folded back and contaminate our spectral density computation. The high frequency that folds back to a low frequency is called an aliase. The aliasing problem sometimes requires a detailed discussion. The aliases of a given frequency λ are $\lambda + 2k\omega_N$, *where* $k = \pm 1, \pm 2, \pm 3, \ldots$ The daily frequency is 7 cycles/week, and for *k*=-3, it is the aliase of +0.82 cycles/week, but the observed peak is at 1/1.2=0.83 cycles/week. Now we are uncertain whether the observed high frequency peak is real at a periodicity 1.2 weeks or it is a contamination from the daily cycle at 1/7 weeks. It is clear that one should formally consider the effect of the Nyquist folding frequency.

Time Domain Analysis - Autoregressive Spectral Analysis

In unpublished work we find a time-domain method (Box-Jenkins model [5]) is used in a meta-analysis of a wide variety of growth time series for differing species, epochs, locations and disease states, as well as media and measures. We use the traditional cosinor analysis of removing a single annual sinusoid by regression and then standardize the remaining residuals to have zero mean and unit standard deviation. Then an autoregessive (AR) model with lags of 3 and 11 is fit in the time domain in order to obtain equivalent of spectral peaks representing the low and high frequency that is the sympathetic and parasympathetic biological rhythms. AR is part of the more general ARIMA (Autoregressive Integrated Moving Average) models used to estimate time series with seasonal components removed. Also the Integrated component is often removed by differencing the time series. We will not consider the Integrated component here, since the integrated component make the time series non-stationary, which is not common in our studies. A model statement for AR of order *k* can be written as:

$$Y(t) = \mu + b_1 Y(t-\Delta) + b_2 Y(t-2\Delta) + \ldots + b_k Y(t-k\Delta) + \sigma\ \epsilon(t),$$

where times are equally spaced multiples of measurement time inteval Δ ($t=j\Delta$), μ and σ are the mean and standard deviation of the series $Y(t)$, $\varepsilon(t)$ is a white noise series (zero mean and unit standard deviation), and coefficients b_1-b_k are constrained so that $Y(t)$ is stationary. Thus, the current value of the time series $Y(t)$ in the time domain is modeled by a linear combination of its past (lagged) values and a current value of error. Fitting these parameters (b_1-b_k, σ^2) by an ARMA procedure (method), we can immediately write down the spectral density $f(\lambda)$ of the time series $Y(t)$ in terms of the estimated parameters.

$$\mathrm{f}(\lambda) = \frac{\sigma^2}{\left|1 - \mathrm{b}_3 \mathrm{e}^{i3\lambda} - \mathrm{b}_{11} \mathrm{e}^{i11\lambda}\right|},$$ where the sinusoid $e^{ix} = cos(x) + i\,sin(x)$, $i = \sqrt{-1}$

and $\lambda=2\pi\Delta$ are spectral frequencies and we plot $f(\lambda)$ as $f(u)$ in terms of $0 \le u \le 0.5$; also we can take $\Delta=1$. Here, the AR model were identified by the auto-correlations (correlation of $Y(t)$ and lagged $Y(t-j\Delta)$), in each time series and can be approximated with only two lags 3 and 11; the rest of the b_j are zero.

This gives spectral peaks; we have attempted to eliminated the peak at $\lambda=0$ by standardization with $\mu=0$ and $\sigma=1$ and the other peaks represent the high and low frequencies. These can be used to numerically compute the low-high ratio (LFHF) of the spectral content (area under the curve in the spectral density) in low and high frequency intervals (0.06,0,22) and (0.32, 0.48), subintervals of the interval $0 \leq u \leq 0.5$.

This method is used here as a meta-analysis for 48 time series from 9 different low and high frequency intervals (0.06,0,22)The computed AR coefficents b_3 and b_{11} are represented here as a scatter plot labeled by source.

This information is better understood in terms the low-high spectral content (LFHF) (Figure 1).

An analysis of variance (ANOVA) of the LFHF outcome does show differences by source (P<0.001) with sources #4 (hydrogen content in mammoth hairs) and #5 (hair growth intervals in young and ancient humans) having higher LFHF ratios. The source factor was chosen to indicate the variety of time series that can be analyzed by autoregressive spectral analysis and not to present important differences that may exist. There are several factors to consider in a multifactor ANOVA: species, disease state, epoch, medium (hair, feathers, teeth), and measure (growth interval, chemical content in equally spaced intervals). This is challenging in terms of experimental design since these factors represent some 72 possible combinations (cells in the design) but we have data for less than half of these cells.

Approximate entropy (ApEen)

The Anthropocene, the man-made world we now live in, is thought to have started ~14,000 years ago; others posit that it began with the industrial revolution from ~1760 AD and continues to this day. This epoch is characterized by ever increasing levels of neuro-toxic metals such as arsenic (As), mercury (Hg), manganese (Mn), and lead (Pb), in the biosphere. But geochemical enrichment evidenced by soil content of such toxins was already detectable ~64 million years ago (MYR), before the advent of humans on earth, in fossil plants. We showed that in highly polluted locations such as modern Lima, Peru, the neurotoxins Hg, Mn, and Pb increased significantly when compared to millennia and decades ago. We attribute this to human activities during the Anthropocene resulting in biological enrichment. We posited that current environmental pollution by humans may have affected health in the recent past and continues to do so at present.

We used approximate entropy (ApEn) to determine the stability of the system derived from our analyses of the metal content in our samples. We found proxies for metal content in the soil in the plants and other biological materials collected from specific sites examined in this study. Evidence for anthropogenic enrichments with neurotoxic metals such as Hg, Mn, Pb, was found in Lima, Peru (Figure 2).

Mercury is a neurotoxin with especially devastating effects on the nervous system. Recent work shows that the emissions of Hg to the biosphere peaked in 1870 but that further additions of Hg occurred in 1970 and although declining until about 2000, the levels of Hg are increasing again. Mercury and other neurotoxins such as Mn, As and Pb at various sites in New Mexico, as examples of less polluted environment, and in Peru, more polluted because of extensive mining activities in the past and more recent further addition of Hg by artisanal mining in some parts of Peru. Lima is a site of considerable anthropogenic enrichment with neurotoxins and high levels of neurotoxins can occur independently of anthropogenic enrichment but the contribution to neurotoxic levels during the Anthropocene is higher than it ever was before.

Reports that plants growing in soil containing gold also contain gold in their leaves support contentions that plants are proxies for metal content of the soil in which they grow. Other biologic sources such as pigeon feathers and wool accumulate neurotoxins through metabolic activity of the animals, for example in Lima, Peru, as shown here. Our results implied that proxies for soil content of neurotoxins could be found in fossil plants; a hypothesis confirmed here in ~64 million year (MYR) old material from the Early Paleocene, Nacimiento Formation in National Conservation Lands near Farmington NM. USA. Thus signatures of enrichments over geologic time scales (geochemical enrichment), before the advent of humans on earth, could be derived from fossil material. Conversely, biologic materials in Lima characterized anthropogenic enrichment due to current human activities.

Evidence from human materials such as bone for lead content has provided estimates of natural lead levels too. These were reported to be some 600-fold lower than what is considered the maximum safe lead level for contemporary children. During the Renaissance bioaccumulation of neurotoxins (Hg and Pb) caused intoxications and death in humans, mostly confined to the nobility who could afford to

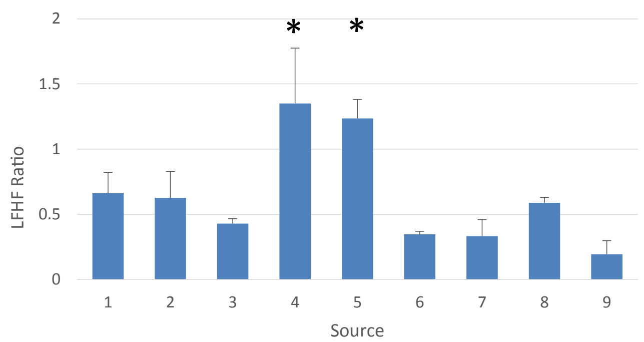

Figure 1: Analysis of variance (ANOVA) of the LFHF outcome does show differences by source.

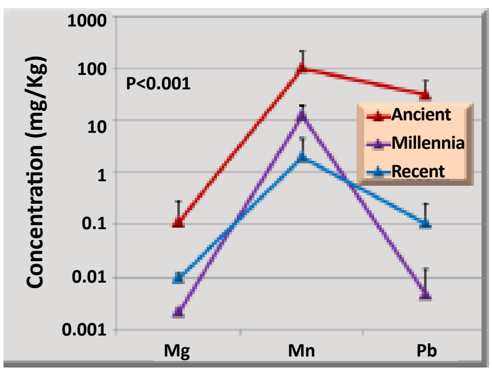

Figure 2: Significantly higher levels of neurotoxins were present in pre-human geochemically enriched biological materials (ancient). We found higher levels of these metals in Lima, Peru than in millennia old and recent material (ANOVA main effect, P<0.001).

drink wine (full of Pb contaminants in the form of sapa, (lead oxide) added as a sweetener) rather than water which, at that time, was heavily contaminated. Similarly, this affluent group could indulge in pharmaceuticals which contained, almost universally at that time, large quantities of Hg. These examples of bioaccumulation-induced diseases underscore the importance of metal content in the biosphere. Sixty four MYR ago, before the advent of humans on earth, there were significantly more neurotoxins in certain locations in New Mexico (geochemical enrichment) but the contents were lower ~120 MYR ago and are still low today. There are significantly more neurotoxins in Lima (anthropogenic enrichment) when compared statistically to the recent past (millennia ago) in other sites in Peru.

The stability of geological and biological systems as expressed by neurotoxin content that define geochemical and anthropogenic enrichments has not changed over geological times. The significance of these findings will emerge after the passage of more time and especially after examination of additional sites in various parts of the globe where such enrichments may be relevant to biology [4].

Tipping points

The first description of children with a previously unrecognized neuropathy in the Four Corners Region of New appeared about 40 years ago. This disease is now named MPV17-related hepatocerebral mitochondrial DNA depletion syndrome (MPV17-NNH). Epidemiological evidence suggested that the disease may run in families; about half the families had more than one affected member. Mean age at death was 10 years. Molecular studies on MPV17-NNH patients showed a single missense mutation in exon 2 in the MPV17 gene (MIM 137960); genetic analyses of unaffected individuals confirmed segregation with the disease.

We examined in this study [7] the heavy metal and neurotoxin content of tissues from patients with MPV17-related hepatocerebral mitochondrial DNA depletion syndrome (MPV17-NNH) (Table 1).

Fossil marine bio-apatite from conodont teeth; small animals that lived in ancient seas, store a record of the content of paleo-seawater of arsenic and lead. These teeth can be compared with teeth from modern humans who have the same apatite composition as that found in conodonts. The arsenic and lead contents in contemporaneous human teeth and can be compared to the amounts of these metals found in ancient rocks [6].

A tipping point is a statistically determined amount reached at which small changes become big enough to cause a large change. In biology the term tipping point refers to oscillating biological systems which cease to oscillate and consequently the organism dies.

Concentrations of As and Pb range approximately from .01 to 100 mg/Kg expressed on a log10 scale (Figure 3). We used statistical methods to compare the tipping points for arsenic and lead in conodonts and contemporaneous human tissue. The tipping point in terms of arsenic (As) and lead (Pb) defines the concentrations of each which would compromise the natural biological rhythms of an animal beyond recovery. The Pb cut score was defined and represents the amount Pb found in human subjects residing in New Mexico [5]. The As cut score is facilitated by the scatter plot of As concentrations versus the Pb concentrations in the samples (Figure 4).

There were enormous levels of Hg (mean 16,000× increase over controls) in the tissues of patients with MPV17-NNH. We also found high levels of other neurotoxins in MPV17-NNH nervous tissues when compared to tissues from subjects not living in the Four Corners region. Arsenic, Cd, Co and Mn were all significantly increased in MPV17-NNH patients. There were very high levels of Hg (mean 16,000 × increase over controls) in the tissues of patients with MPV17-

Metals	Mean	SE
As	18.2	5.6
Cd	9.8	1.9
Co	2.5	0.72
Mn	2.3	0.51
Pb	0.28	0.09
U	0.30	0.17
Hg	16,300	11,700

Table 1: Mean values (±SE) of metal ratios MPV17-NNH/control tissues. Mercury was approximately 16,000 times higher in MPV17-NNH nervous tissue.

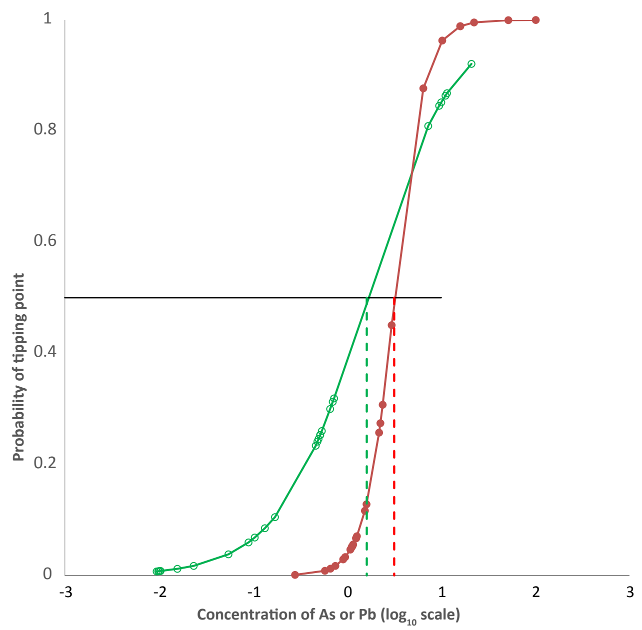

Figure 3: Probability of exceeding a tipping point versus concentration of As (green curve) or Pb (red curve).

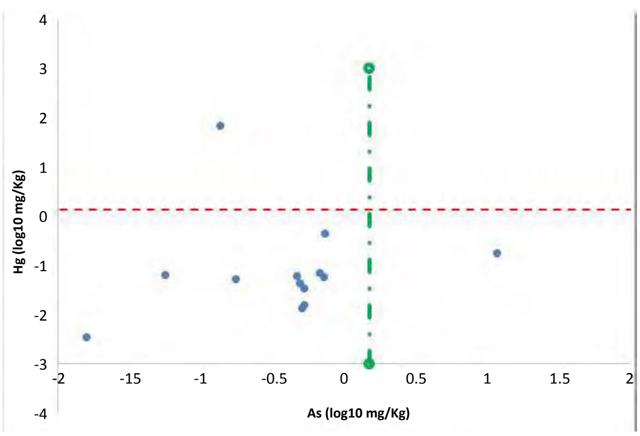

Figure 4: Hg log_{10} concentration versus As log_{10} concentration in brain and nerve tissues (blue solid circles). Dashed lines denote Hg tipping point (red) and As tipping point (green). Four-corner region-USA is far beyond Hg tipping point and Chile is beyond the As tipping point.

NNH. The large variations (SD) in tissue Hg content were the results of including liver tissue (one pre-transplantation cirrhotic liver) in our analysis. We also found high levels of other neurotoxins in MPV17-NNH nervous tissues when compared to tissues from subjects not living in the same area. Arsenic, Cd, Co and Mn were all significantly increased in MPV17-NNH. We have compelling but circumstantial evidence, therefore, which suggests that metals in the biosphere of the Four Corners region of NM, USA may contribute to shortened life-span in that region of the population in general and of patients with MPV17-NNH in particular. Thus this suggests that patients with this disease had reached the tipping point which caused their demise at an average age of 10 years.

Another variant of tipping points can be found in historical accounts of the lack of health in the royal couple Ferrante II (1469-1496) and Isabella (1470-1524) of Aragon. These symptoms together with evidence a heavy metal (lead or mercury) load were used to define paleo-clinical symptom score; thus a symptom score of 50 or lower represent a tipping point where heavy metal toxicity might lead to irreversible collapse of an individual's metabolism. This was shown in a contour plot. There is good evidence for the presence of lead being found in Ferrante's bone and of mercury in Isabella. Ferrante, who probably had an high lead intake since early childhood, showed the ravages of lead on autonomic nervous system (ANS) function evidenced by his significantly shortened annual hair growth rate and alteration of the power spectra derived from hydrogen isotope ratios along the length of his hair.

The spectra derived from hydrogen isotope ratios are used to compute an annual hair growth rate of 12 cm/year for Ferrante and 2 cm/year for Isabella. Both are disrupted from the normal 16 cm/year and Isabella's growth rate is extreme suggesting her death was related to mercury toxicity whereas Ferrante's early death was not related - his death was attributed to "malignant tertian malaria". The high frequency/low frequency ratios computed as power from the spectra indicate that both had disrupted biological rhythms consistent with the effect of heavy metals on the ANS. Of interest, the slower growth rate in hair can by explain by longer durations of telogen (quiescence periods).

Low frequency to high frequency spectral content

Hummingbirds show remarkable adaptations to mountainous environments in the Americas. Although the hummingbird clade originated in the lowlands, some species are resident up to ~5000 m, similar in elevation to the highest permanent human dwelling.

Acute adaptation to altitude requires autonomic nervous system (ANS) adjustments to cope with short term environmental influences such as ambient hypoxia and low temperatures. However, long-term survival at altitude depends on additional adaptive strategies that modify metabolism and hemoglobin levels.

More than 2 million people are born, live, work and adapt to altitude in the Andes, East African high altitude plateau, and Himalayas but they cope with the ambient stress of altitude life in different ways and with varying success. One way to adapt to altitude is by increasing the hemoglobin content of the blood to improve oxygen uptake and delivery to tissue. Additional short-term adaptive mechanisms depend on changes in autonomic nervous system function (ANSf) such as thermoregulation and respiratory function. Many genetic and physiologic mechanisms have been discovered that also contribute to the success or failure of human adaptation to altitude, however, no evidence of maladaptation in hummingbirds has been reported to date.

Altitude adapted hummingbirds might exhibit differences in hemoglobin content, metabolism, and autonomic nervous sytem function when compared to human altitude dwellers. We used field measurements of hemoglobin concentration in humming birds and museum measurements of growth rhythms (scale bars for metabolism) in hummingbird tail feathers to model altitudinal patterns of variation in human and hummingbirds metabolism.

We used hummingbird specimens from the Museum of Southwestern Biology of the University of New Mexico to measure growth bar-intervals which reflect the growth of the tail feathers on rectrices (Figure 5). We obtained measurements from 1024 individual hummingbirds, representing 72 species, We used hemoglobin concentration estimates from a total of 6561 individual humans from altitude populations residing in the Andes, Himalayas and Ethiopia previously published [9-11].

We gauged autonomic nervous system function derived from the ratios of low/high frequencies (LF/HF) from spectral analyses of growth intervals of hummingbird feathers measured in 1173 feathers (53 individual birds), 94 non-avian theropod rock imprints of feathers and 23 non-avian theropod rock imprints.. Additionally we measured 46 rachis growth-intervals. We also included in the analyses oxygen hydrogen ratios measured along the length of the hairs (a measure of growth and metabolism) from 8 humans; 1 horse tail hair and a hair from 1 Siberian mammoth to generate the power spectra.

We used the measured width of the combined dark and light banding on hummingbird feathers as a proxy for 24-hour growth and metabolism (Figure 5).

Hemoglobin levels were higher in hummingbirds (P<0.001) than in humans, but the influence of altitude on hemoglobin was more pronounced in humans (slope, P<0.001).

We confirmed an increased mass of hummingbird at altitude. The width of the sum of the dark and light bands of hummingbird tail feathers; a proxy for metabolic rhythms, did not change with altitude [9,10].

We analyzed Hummingbird mass versus altitude and altitude temperature and show the dark and light bands in a hummingbird tail feather (Figure 5).

Figure 5: Distinctive light and dark banding in hummingbird tail feather. The dark band is a product of daylight metabolism; the light band accretes at night. The feather in the figure is from a specimen of Patagona gigas. The scale bar visible in the left upper corner of the image indicates length in mm.

We developed statistics related to ratio (LF/HF) of low frequency to high frequency spectral content (areas under the curve of the spectrum, AUC). The basic distributional theory is given in Qualls and Appenzeller [3] and in [12]. We have from equations 6, 8, and 9 that the ratio LF/HF is a random variable with a distribution proportional to an F-distribution. The assumptions were normality or large samples, and disjoint frequency bands for the calculations of AUC1 and AUC3, which nearly give independence of these two AUCs. The subscripts 1, 3 are arbitrary, though they refer to three bands of frequencies, low, mid. and high, where the band of mid frequencies, labeled 2, are left out of the computation of the ratio. In particular,

$$LFHF = \frac{AUC_1}{AUC_3} \sim \frac{c_1 R_1}{c_3 R_3} * F_{R_1, R_3} \ ,$$

where F_{R_1,R_3} is a F statistic with degrees of freedom R_1,R_3 and

$$R_i = 2\frac{E^2(AUC_i)}{Var(AUC_i)} \text{ and } c_i = \frac{1}{2}\frac{Var(AUC_i)}{E(AUC_i)} \quad for \ i = 1,3.$$

Here E is expectation and Var is variance of the random variable AUC_i.

Note $c_i R_i = E(AUC_i)$; thus, a point estimate of $c_i R_i$ and $E(AUC_i)$ is AUC_i and a likelihood estimate of

$$\frac{c_1 R_1}{c_3 R_3} \ is \ \frac{AUC_1}{AUC_3} = \ LFHF.$$

The computation of the first and second moments $E(AUC_i)$ *and* $Var\ (AUC_i)$ are adapted from Priestley [12] and are given, Also note that the F-distribution used here is generalized in that the degrees of freedom R_i are not necessarily integers.

The F-distribution can be used to give a 95% confidence interval for LFHF:

$$P\left[\frac{c_1 R_1}{c_3 R_3} * F^{-1}_{R_1,R_3}(.025) \le \frac{c_1 R_1}{c_3 R_3} * F_{R_1,R_3} \ \le \frac{c_1 R_1}{c_3 R_3} * F^{-1}_{R_1,R_3}(.975)\right] = 0.95 \ \text{ or,}$$

$\left(LFHF * F^{-1}_{R_1,R_3}(.025)\ ,\ LFHF * F^{-1}_{R_1,R_3}(.975)\right)$ is a 95% confidence interval of the expected value of *LFHF*.

Here $F^{-1}_{R_1,R_3}(.025)$ *and* $F^{-1}_{R_1,R_3}(.975)$) are the 2.5 and 97.5 percentiles of this F-distribution to be computed from an F-table or by computer program.

Next we compute the error bars of LF/HF for graphical purposes. For symmetric error bars and based on the variance of the F-distribution. We have

$$Standard\ error\ SE = \sqrt{Var\left[\frac{c_1 R_1}{c_3 R_3} * F_{R_1,R_3}\right]} = \frac{c_1 R_1}{c_3 R_3}\ \sqrt{Var\left[F_{R_1,R_3}\right]}, \text{ thus}$$

$$SE = \ LFHF * \sqrt{2\frac{R_3^2\ (R_1 + R_3 - 2)}{R_1(R_3-2)^2\ (R_3-4)}}\ , provided\ R_3 > 4.$$

If one allows asymmetric error bars, then one could use the 68% content interval (mean ±SE is a 68% interval for the normal distribution) as follows.

$$LFHF * \left(F^{-1}_{R_1,R_3}(0.16), F^{-1}_{R_1,R_3}(0.84)\right).$$

Example: Our collection of humming birds provided measurement of alternating light and dark bands in feathers. The widths of dark bands reflect metabolism during daylight and form a time series (529 observations) suitable for spectral analysis. Since these humming birds live and were collected at known altitudes, we are able to compute LF/HF ratios as a function of altitude. Using SAS 9.4, PROC SPECTRAL, and data step programming, we compute the parameters mentioned above from the spectra of the dark band series for humming bird feathers at specific altitudes (detailed altitudes were pooled into representative categories of 0, 1500, 3000 and 4500 meters) (Table 2).

For the differences in LF/HF at different altitudes for humming birds, we use t-tests. There were no significant differences (all P>0.15). Similarly, for humans, there were no significant differences in LF/HF (all P>0.22).

In growing tissues such as feathers, the growth bars are easily discernible by their repetitive patterns, visible in the dark and light bands shown in the feather (Figure 6) We focused our attention on the dark bands because they reflect metabolism during the day, whereas the light band grows during the night, a time when most hummingbirds at altitude go into torpor (a state of physical inactivity).

Humans living at altitude exhibit genetically based physiological adaptations to allow prolonged survival above 2500 m, at least some of which relate to blood hemoglobin concentration [8]. Such adjustments are not always capable of ensuring a healthy existence. However, evolution often conserves successful adaptive strategies and uses these repeatedly and in different species. This study implies that unlike variation among human individuals and populations, variation in hemoglobin among hummingbird species increases only subtly with increasing altitude. However, at extreme altitudes, human hemoglobin approaches that of hummingbirds (~19 g/dl); (Figures 6 and 7).

The red dot on the *Y* axis signifies the range of normal human hemoglobin values at sea level (13.5-17.7 g/dL the levels also vary by age and sex). Blue points are mean values of hemoglobin and elevation for each hummingbird species, whereas the red points are for one species (human).

This phenotypic convergence is remarkable considering the contrasting evolutionary histories of these two taxa at altitude. Humans colonized high altitude thousands of years ago and maintained gene

alt alt_1500_1500	total123	sum1	sum2	sum3	LFHF12	LFHF13	
0	0.99	0.65	0.19	0.16	3.43	4.12	
1500	1.02	0.36	0.27	0.39	1.35	0.91	
3000	0.99	0.46	0.23	0.31	2.01	1.51	
4500	0.99	0.60	0.18	0.21	3.23	2.78	
alt_1500	**sig1**	**sig2**	**sig3**	**R1**	**R3**	**SE_F**	**SE_LFHF**
0	0.28	0.054	0.035	10.7	39.5	0.53	2.19
1500	0.14	0.082	0.094	12.7	35.4	0.51	0.46
3000	0.19	0.073	0.074	11.9	33.6	0.53	0.80
4500	0.22	0.060	0.048	15.0	40.5	0.46	1.29

Table 2: Our collection of humming birds provided measurement of alternating light and dark bands in feathers.

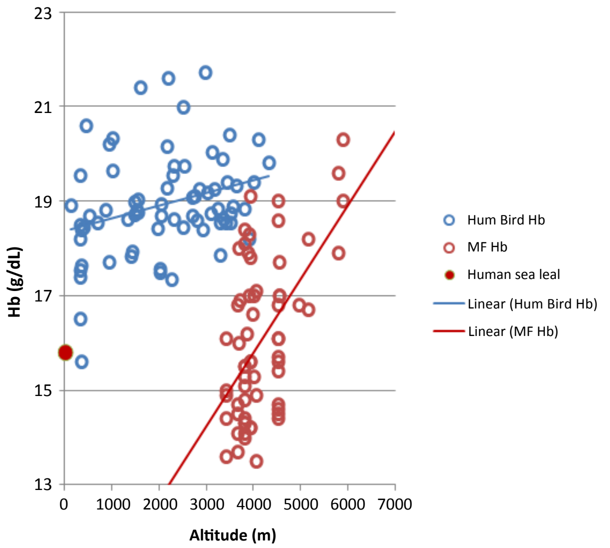

Figure 6: Effect of altitude on Hemoglobin (Hbg) in hummingbirds (blue) and humans (red).

Figure 7: Several healed burr holes made during life of this individual.

flow between high and low altitude populations in contrast, several lineages within the hummingbird clade colonized altitude millions of years ago and gave rise to numerous high-altitude specialist species that long ago stopped exchanging genes with lowland relatives.

Conclusion

All growing tissues, such as teeth, bone, and hair, reflect metabolism of the animals in which they are examined. Growth is costly in terms of energy used; therefore, to grow necessitates an increase in food consumption to meet the energy demands of increased metabolism and body mass. We derived metabolism from growth intervals of hummingbird feathers and, a variety of other growing tissues such as human and animal hairs, and dinosaur rock imprints of their feathers. We show that altitude has no discernible effect on hummingbirds' metabolic adjustments to ambient conditions as judged from their feather's growth. Although hummingbird species living at higher altitudes are generally heavier than their lowland relatives, there is extensive overlap among constituent species in highland and lowland communities. By contrast humans, lifelong exposure to altitude requires considerable metabolic adjustments, aided by steeper altitude related increases in blood hemoglobin content in Highlanders and generally smaller stature than lowlanders. Our results support the notion that hummingbird hemoglobin levels and metabolism are useful models for the study of biologically adaptive strategies to life in ambient hypoxia.

Hummingbird thermoregulation has been examined. Remarkably, because of their flying style, they generate enormous amounts of heat. To sustain metabolism for hovering in the hypodense air, hummingbirds must increase their food intake and enlarge their wing-span which, in turn, results in increased body mass at altitude as observed in this study. At low altitudes, feeding times in this taxon can be limited by high temperatures, necessitating frequent rest periods to allow for cooling. At altitude, decreased ambient temperatures might increase the available time for feeding and this could have been an additional factor in the evolutionary expansion of hummingbirds to high altitude and subsequent adaptation. Furthermore, the ability of hummingbirds to use the nightly torpor to conserve energy during inactive periods could be another pre-adaptation to altitude. By contrast, although humans face less severe thermal constraints due to their larger body sizes, and microclimate provided by clothing, recent genetic studies have revealed the possibility that high-latitude, as well as cold-adapted alleles, may have pre-adapted humans to colonize high-altitude habitats.

In hummingbirds adaptation to altitude is also aided by amino-acid substitutions in hemoglobin that improve oxygen uptake and delivery at altitude by increasing O_2-binding affinity. Functional amino acid substitutions in hemoglobin also occur in many other altitude vertebrates who live at high altitudes. However, there is no good evidence to date that any of those variants enhance respiratory function at altitude or provide a fitness advantage under any circumstances.

References

1. Qualls C, Costa MA, Paffett M, Appenzeller O (2017) Tooth Growth in Ancient and Modern Times Inferred from Perikymata Growth Intervals; Modeled Statistically. J Biom Biostat 8: 1-5.
2. Appenzeller O, Stevens JM, Kruszynski R, Walker S (2001) Neurology in ancient faces. J Neurol Neurosurg Psychiatry 70: 524-529.
3. Qualls C, Appenzeller O (2015) Modeling Metabolism and Disease in Bioarcheology. Biomed Res Int 2015: 1-8.
4. Qualls C, Lucas SG, Spilde M, Appenzeller O (2016) Biological Rhythms, Metabolism and Function in Feathered Dinosaurs; As Determined by Biostatistics. J Biom Biostat 7: 326.
5. Box GEP, Jenkins GM (1970) Time series analysis: forecasting and control. CA: Holden-Day, San Francisco, p: 56.
6. Qualls C, Ali A, Lucas SG, Lombardi G, Appenzeller O (2016) Geochemical and Biological Enrichments with Toxic Metals; Anthropogenic Effects. J Environ Anal Toxicol 6: 419.
7. Qualls C, Kornfeld M, Joste N, Ali A, Appenzeller O (2016) MPV17-related hepatocerebral mitochondrial DNA depletion syndrome (MPV17-NNH) revisited. eNeurologicalSci 2: 8-13.
8. Qualls C, Lucas SG, Ali A, Appenzeller O (2018) Tipping Points; a Statistical Comparison between Humans and Conodonts. J Biom Biostat 9: 398.
9. Qualls C, Witt CC, Wilson NR, Cruz SR, Bautista E, et al. (2017) Human and Hummingbird Hemoglobin Concentrations and Metabolic Rhythms at Altitude Determined with Statistical Modeling. J Biom Biostat 8: 373.
10. Wu TY, Liu FY, Ouzhou-Loubu, Cui CY, Qi XB, et al. (2013) A genetic adaptive pattern-low hemoglobin concentration in the himalayan highlanders. Chin J Appl Physiol 29: 481-493.
11. Grubb TC (2009) Ptilochronology: Feather time and the biology of birds. Oxford University Press 15: 159.
12. Priestley MB (1992) Spectral Analysis and Time Series, vol. 1, Academic Press. San Diego, CA. 1981, 7th Printing with corrections, p: 427.
13. Jordanov J, Dimitrova B, Nikolov S (1988) Symbolic trepanations of skulls from the Middle Ages (IXth-Xth century) in Bulgaria. Acta Neurochir (Wien) 92: 15-18.
14. Spilde M, Lanzirotti A, Qualls C, Phillips G, Appenzeller O (2011) Biologic rhythms derived from siberian mammoths' hairs. PLoS One 6: e21705.